

A new scheme for short baseline electron antineutrino disappearance study

Jae Won Shin¹, Myung-Ki Cheoun¹, Toshitaka Kajino² and Takehito Hayakawa³

¹ Department of Physics and Origin of Matter and Evolution of Galaxies (OMEG) Institute, Soongsil University, Seoul 156-743, Korea

² Division of Theoretical Astronomy, National Astronomical Observatory of Japan, Mitaka, Tokyo 181-8588, Japan

and Department of Astronomy, Graduate School of Science, University of Tokyo, Hongo, Bunkyo-ku, Tokyo 113-0033, Japan

³ Quantum Beam Science Directorate (QUBS), Japan Atomic Energy Agency (JAEA), 2-4 Shirane, Shirakata, Tokai-mura, Naka-gun, Ibaraki 319-1195, Japan

E-mail: cheoun@ssu.ac.kr (Corresponding Author)

1 Aug. 2017

Abstract. A new scheme for the short baseline electron antineutrino ($\bar{\nu}_e$) disappearance study is investigated. We propose to use an intense neutron emitter, ^{252}Cf , which produces ^8Li isotope through the $^7\text{Li}(n,\gamma)^8\text{Li}$ reaction; ^8Li is a $\bar{\nu}_e$ emitter via β^- decay. Because this $\bar{\nu}_e$ source needs neither accelerator nor reactor facilities, the $\bar{\nu}_e$ can be placed on any neutrino detectors as closely as possible. This short baseline circumstance with a suitable detector enables us to study the existence of possible sterile neutrinos, in particular, on 1 eV mass scale. Also, complementary comparison studies among different neutrino detectors can become feasible by using $\bar{\nu}_e$ from the ^8Li source. As an example, applications to hemisphere and cylinder shape scintillator detectors are performed in detail with the expectation signal modification by the sterile neutrino. Sensitivities to mass and mixing angles of sterile neutrinos are also presented for comparison with those of other neutrino experiments.

PACS numbers: 26.65.+t, 14.60.Pq, 24.10.Lx, 02.70.Uu

Keywords: Short baseline neutrino disappearance, Electron antineutrino source, Sterile neutrinos

Submitted to: *J. Phys. G: Nucl. Part. Phys.*

One of open issues in the particle and neutrino physics is the existence of hypothetical fourth neutrino which may be mixed with active neutrinos [1]. This fourth neutrino, so-called sterile neutrinos (ν_s), is claimed to play important roles of explaining some anomalies reported in LSND [2], MiniBoone [3], reactor experiments [4], and gallium experiments [5]. A few experiments with compact neutrino detectors and reactor facilities [6, 7, 8, 9, 10, 11] or antineutrino sources from radioactive isotopes [12, 13, 14] or an accelerator-based IsoDAR (isotope decay-at-rest) [15, 16, 17] are proposed to search the existence of ν_s .

By using compact neutrino detectors such as DANSS [6], NEUTRINO4 [7], NUCIFER [8], PANDA [9], PROSPECT [10], and STEREO [11], experiments have been planned to measure reactor neutrinos at a distance of several meters. KamLAND (CeLAND) [13] and Borexino (SOX) [14] plan to perform experiments by using antineutrino generators of unstable isotopes ^{144}Ce - ^{144}Pr of a radioactivity of 100 kCi, where neutrino energies are lower than 3 MeV. As another type of antineutrino source, ^8Li was suggested by using an accelerator-based IsoDAR concept [16, 17]. Electron antineutrinos ($\bar{\nu}_e$) were assumed to be emitted from ^8Li through β^- decay with energies of up to ~ 13 MeV. Because these energies are higher than those from ^{144}Ce - ^{144}Pr , ^8Li can be used for study of $\bar{\nu}_e$ spectrum distortion in the energy region of $5 \text{ MeV} < E_{\bar{\nu}} < 7 \text{ MeV}$, where some distortions or anomalies were reported by reactor antineutrino experiments (Daya Bay [18], Double Chooz [19] and RENO [20, 21]).

In this letter, as a new ^8Li generator, we propose a fissionable isotope of ^{252}Cf radioactive isotope-based $\bar{\nu}_e$ production scheme. In particular, our ^8Li generator can be placed on any neutrino detectors such as Borexino [22], JUNO [23], KamLAND [24], LENA [25] and SNO+ [26], etc., because one does not need any accelerator or reactor systems. As an intense neutron emitter, ^{252}Cf is used for productions of ^8Li . ^{252}Cf with a half-life of 2.64 yr emits neutrons with an average energy of 2 MeV via spontaneous fissions. The neutron emission rate of 1 gram of ^{252}Cf is 2.34×10^{12} neutrons per second (n/s). For energy distribution of neutrons from ^{252}Cf we take Watt fission spectrum [27, 28, 29] in this work.

We consider three different types of geometrical setups for productions of ^8Li as shown in Fig. 1. Figure 1 (a, d) (setup I) shows a simple setup case with 99.99% enhanced ^7Li convertor and ^{252}Cf surrounded by the Li convertor.† The Li convertor has a cylindrical shape of a radius of 100 cm and a length of 200 cm based in Ref. [16]. In Fig. 1 (b, e) (setup II), we add carbon (graphite) material as a neutron reflector to the setup I. The carbon is preferred as the neutron reflector due to its low absorption cross section and high elastic scattering cross section. This concept is known as the Adiabatic Resonance Crossing (ARC) [30] for the transmutation of long-lived radio isotopes in the nuclear waste and the medical radioisotope production [31, 32, 33]. With the carbon reflector, we can increase production yield of ^8Li even though the amount of ^7Li is less than that of the setup I. The setup III in Fig. 1 (c, f) has two carbon reflectors. One is

† A ^{252}Cf source is enclosed with the stainless steel case, but the presence of the case does not affect present work.

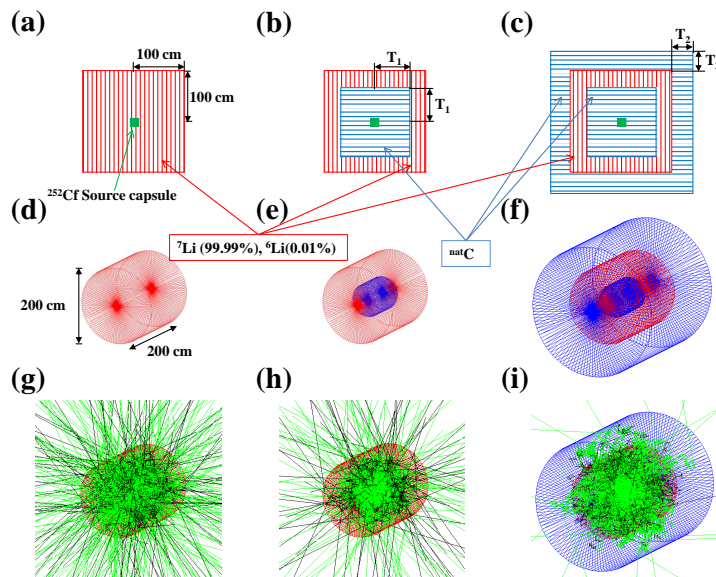


Figure 1. (Color online) Schematic horizontal cross section views (a, b, c) of three different cylindrical ${}^8\text{Li}$ generator types (d, e, f), referred as setup I, II and III, respectively. Simulation snapshots by OpenGL pictures for the ${}^8\text{Li}$ generators with ${}^{252}\text{Cf}$ source are shown at the lowest panel (g, h, i). Green and black lines stand for neutrons and γ , respectively.

surrounded by the Li convertor and another wraps the Li convertor.

The production rate of ${}^8\text{Li}$ by neutrons from ${}^{252}\text{Cf}$ is estimated by using GEANT4 code (v. 10.1) [34, 35]. High precision models with G4Neutron Data Library (G4NDL) 4.5 are used in the present work. The data in G4NDL 4.5 come largely from the Evaluated Nuclear Data File (ENDF/B-VII) library [36]. Simulation snapshots for the ${}^8\text{Li}$ generator setup I, II, and III are shown in Fig. 1 (g, h, i), respectively. § For the setup I, neutrons and γ rays easily escape from the neutrino source, while the numbers of neutrons and γ escaping from the setup II and III are drastically reduced by the carbon reflectors.

First, we calculate the production yield of ${}^8\text{Li}$ for the case of setup I depicted in Fig. 1 (g), and obtain the yield of 0.0045 ${}^8\text{Li}$ per neutron (${}^8\text{Li}/\text{n}$). The production yields of ${}^8\text{Li}$ for the setup II and III are sensitive to the thickness of carbon reflector, T_1 and T_2 , in Fig. 1. As the thickness of the reflector increases, numbers of the collisions between the neutron and the carbon also increase. Thus, probabilities for the neutron capture by ${}^7\text{Li}$ can also increase. If the T_1 is too thick, however, it becomes hard for the scattered neutron to escape from the inner carbon, namely, these neutrons are rarely absorbed to ${}^7\text{Li}$.

Figure 2 (a) shows the dependence of the ${}^8\text{Li}$ yields on the thickness of carbon reflector (T_1) for setup-II. Yields of ${}^8\text{Li}$ increase when T_1 increases up to 43 cm. Maximum yield of ${}^8\text{Li}$ is 0.157 ${}^8\text{Li}/\text{n}$ at $T_1 = 43$ cm, where the yield is larger than

§ For simplicity, simulations have been performed with 500 neutrons generation from ${}^{252}\text{Cf}$ where the neutron has a Watt fission spectrum in Refs. [27, 28, 29].

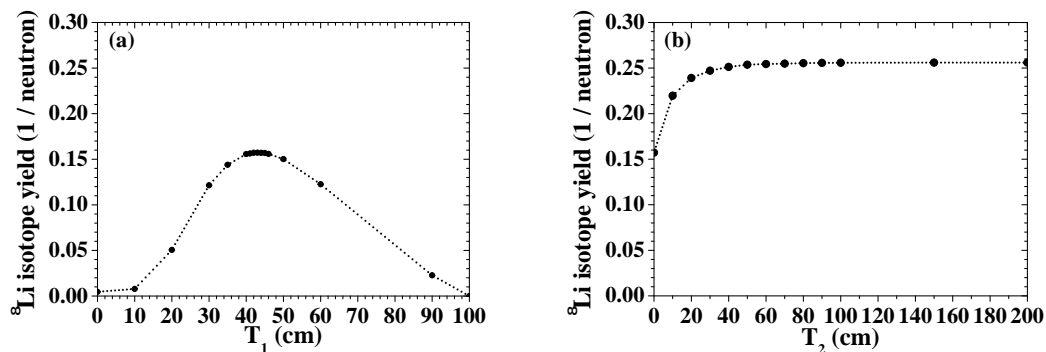


Figure 2. (Color online) (a) ${}^8\text{Li}$ isotope yields for setup II with respect to T_1 . (b) ${}^8\text{Li}$ isotope yields for setup III with respect to T_2 , where T_1 is set to be 43 cm which is a optimal thickness in (a).

those for setup-I about 35 times. As the T_1 increases more than 43 cm, yields of ${}^8\text{Li}$ decrease. In Fig. 1 (h), un-captured neutrons by ${}^7\text{Li}$ still can escape from the geometry. To further increase the yields of ${}^8\text{Li}$, additional carbon reflector with the thickness T_2 is considered to be located out of the Li convertor.

The production yield for ${}^8\text{Li}$ with respect to T_2 is plotted in Fig. 2 (b). Figure 2 (a) shows that the optimal thickness of T_1 is 43 cm, and thus the same thickness is chosen for setup-III. As the T_2 increases, ${}^8\text{Li}$ yields also increase up to 0.256 ${}^8\text{Li}/\text{n}$. With the T_2 larger than 50 cm, yields for ${}^8\text{Li}$ are almost saturated. Maximum yields of ${}^8\text{Li}$ for setup-III are larger than those for setup-II and setup-I by factors ~ 1.6 and ~ 56.9 , respectively.

We obtained a result that the yields of ${}^8\text{Li}$ increase to the maximum value at $T_1 = 43$ and $T_2 = 100$ cm of the setup III, where the production yield is 0.256 ${}^8\text{Li}/\text{n}$. ${}^8\text{Li}$ with a half-life of 0.838 s emits $\bar{\nu}_e$ through β^- decay. The electron anti-neutrinos from ${}^8\text{Li}$ have continuous energy distribution, which is evaluated by using “G4RadioactiveDecay” [37, 38] class based on the Evaluated Nuclear Structure Data File (ENSDF) [39].

Electron antineutrinos can be measured with two different neutrino reactions. One is $\bar{\nu}_e$ elastic scattering on electrons (ES), and another is inverse beta decay (IBD) reaction, $\bar{\nu}_e + p \rightarrow e^+ + n$. In ES, $\bar{\nu}_e$ can be indirectly measured by the scattered e^- by liquid-scintillator (LS). Expected event rate for ES can be obtained from Refs. [40, 41]. The event rate ($R_{\bar{\nu}_e}^{IBD}$) for IBD is written as

$$R_{\bar{\nu}_e}^{IBD} = n_p \int_{E_{th}}^{E_{max}} dE_{\bar{\nu}} \Phi_{\bar{\nu}_e}(E_{\bar{\nu}}) P_{\nu\bar{\nu}}(E_{\bar{\nu}}) \sigma_{\bar{\nu}_e}^{IBD}(E_{\bar{\nu}_e}), \quad (1)$$

where n_p is the number of target protons within a fiducial volume of the detector, $\Phi_{\bar{\nu}_e}(E_{\bar{\nu}})$ is the $\bar{\nu}_e$ flux from ${}^8\text{Li}$, $P_{\nu\bar{\nu}}(E_{\bar{\nu}})$ is the energy dependent $\bar{\nu}_e$ survival probability. The energy dependent cross section of IBD is approximately taken by [42]

$$\sigma_{\bar{\nu}_e}^{IBD}(E_{\bar{\nu}_e}) \approx p_e E_e E_{\bar{\nu}_e}^{-0.07056+0.02018 \ln E_{\bar{\nu}_e} - 0.001953 \ln^3 E_{\bar{\nu}_e}} \times 10^{-43} [\text{cm}^2], \quad (2)$$

where p_e , E_e , and $E_{\bar{\nu}_e}$ are the positron momentum, total energy of the positron, and

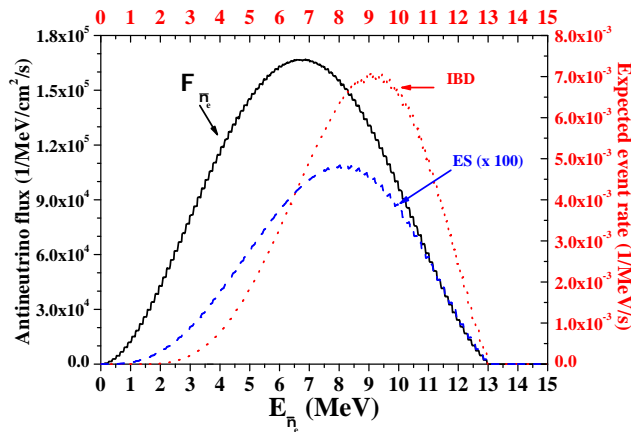


Figure 3. (Color online) $\bar{\nu}_e$ flux from ${}^8\text{Li}$ source and expected event rates for ES and IBD. Here we assumed 1 g of ${}^{252}\text{Cf}$ in the setup III and detector at 2 m from the neutrino source. The black solid line is the electron-antineutrino energy spectrum. The red dotted line and the blue dashed line are the event rates for IBD and ES, respectively. For ES, we multiply 100 to the rate.

energy of $\bar{\nu}_e$ in MeV, respectively.||

In Fig. 3, energy distribution of $\bar{\nu}_e$ from ${}^8\text{Li}$ and expected event rates of ES and IBD are presented, where ${}^8\text{Li}$ is assumed to be produced by the setup III. For the calculation of neutrino oscillation, we use the $P_{\nu\bar{\nu}}(E_{\bar{\nu}})$ ($\equiv P_3$) given by [43]

$$P_3 = 1 - \sin^2 2\theta_{13} S_{23} - c_{13}^4 \sin^2 2\theta_{12} S_{12}, \quad (3)$$

where $S_{23} = \sin^2(\Delta m_{32}^2 L/4E)$ and $S_{12} = \sin^2(\Delta m_{21}^2 L/4E)$. Neutrino oscillation parameters are taken from a global fit from Ref. [44]. For comparison, we chose the number of electrons (n_e) in LS for ES as the same as the numbers of protons (n_p) in LS for IBD. The reaction rates of ES turn out to be much smaller than those of IBD. Therefore, herefrom we only consider IBD for the following neutrino disappearance study.

The IBD reaction offers two signals in neutrino detections; one is a prompt signal due to annihilation of a positron, and another is a delayed signal of 2.2 MeV γ ray via a neutron capture, which provides almost unambiguous antineutrino event detection. The two distinct detections give an efficient rejection of other possible backgrounds.

Note that various unstable isotopes which emit antineutrinos can be produced. In the Li convertor, ${}^3\text{H}$, ${}^6\text{He}$, and ${}^{10}\text{Be}$ are produced as well as ${}^8\text{Li}$. However, ${}^3\text{H}$ decays with a half-life of 12.3 y, and the production yields of ${}^6\text{He}$ and ${}^{10}\text{Be}$ are much lower than that of ${}^8\text{Li}$ by factors of 10^4 and 10^7 , respectively. ${}^{10}\text{Be}$, ${}^{12}\text{B}$, and ${}^{14}\text{C}$ are produced in the carbon reflectors. Due to low yields of ${}^{10}\text{Be}$ and ${}^{12}\text{B}$ and a long half-life of ${}^{14}\text{C}$ (5.7×10^3 y), their contributions are marginal for the IBD neutrino detections.

There are background neutrinos such as neutrinos from fission product of ${}^{252}\text{Cf}$ (ν_f)

|| This cross section agrees within few per-mille with the full calculation including the radiative corrections and the final-state interactions in IBD.

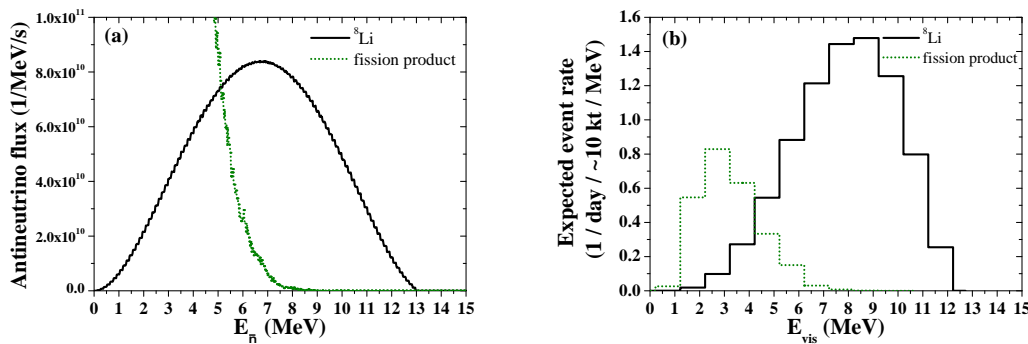


Figure 4. (Color online) $\bar{\nu}_e$ flux (a), which is total flux of that in figure 3, and expected event rates (b) for ${}^8\text{Li}$ and fission product of ${}^{252}\text{Cf}$. The black solid lines denote the electron-antineutrino from ${}^8\text{Li}$ and the green dotted lines represent those from fission product of ${}^{252}\text{Cf}$.

and geo-neutrinos (ν_{geo}). To see the effect of the ν_f , we estimate flux and event rate for ν_f by using ENDF/B-VII and ENSDF data, and the results are compared with those from ${}^8\text{Li}$ ($\nu_{{}^8\text{Li}}$) in Fig. 4. Figure 4 (a) shows that the ν_f are dominant in low energy regions. However, for $E_{\bar{\nu}_e} > 7$ MeV (corresponding to $E_{vis} > 6.22$ MeV), contributions of the ν_f are negligible compare to the $\nu_{{}^8\text{Li}}$. Total expected event rate of ν_f for $E_{\bar{\nu}_e} > 7$ MeV in Fig. 4 (b) is smaller than those from ${}^8\text{Li}$ by three orders of magnitudes. With the neutrino energy cut of 7 MeV, we can remove the effect of ν_f in our work. KamLAND [45] and Borexino [46, 47] have measured a rate for ν_{geo} . (\sim a few events/(100 ton \cdot yr)) due to the decay of U or Th in the Earth. Contributions of the ν_{geo} is negligible compare to those of $\bar{\nu}_e$ from ${}^8\text{Li}$.

Electron-antineutrino survival probabilities in Eq. (1) by the 3+1 and 3+2 scenarios can be written as [16]

$$P_{3+1} = 1 - 4|U_{e4}|^2(1 - |U_{e4}|^2)\sin^2(\Delta m_{41}^2 \frac{L}{4E}), \quad (4)$$

$$P_{3+2} = 1 - 4[(1 - |U_{e4}|^2 - |U_{e5}|^2) \times (|U_{e4}|^2 \sin^2(\Delta m_{41}^2 \frac{L}{4E}) + |U_{e5}|^2 \sin^2(\Delta m_{51}^2 \frac{L}{4E})) + |U_{e4}|^2 |U_{e5}|^2 \sin^2(\Delta m_{54}^2 \frac{L}{4E})], \quad (5)$$

where relevant parameters are taken from the best-fit points for the 3+1 and 3+2 scenarios from the reactor antineutrino data at Table 1 in Ref. [48].

The visible energy (E_{vis}) of the prompt signal due to a positron (e^+) is strongly correlated with the energy of $\bar{\nu}_e$ ($E_{\bar{\nu}_e}$), $E_{\bar{\nu}_e} \simeq E_{vis} + 0.78$ MeV, by which $\bar{\nu}_e$ energy spectrum can be reconstructed using E_{vis} . The spectral shape of E_{vis} would give a valuable chance to check the existence of the fourth neutrino. To see the effect of ν_s using the shape analysis like Double Chooz, Daya Bay, and RENO experiments, event rates are estimated for two different types of LS detectors based on the JUNO [23] and the LENA [25] with respect to E_{vis} in the following.

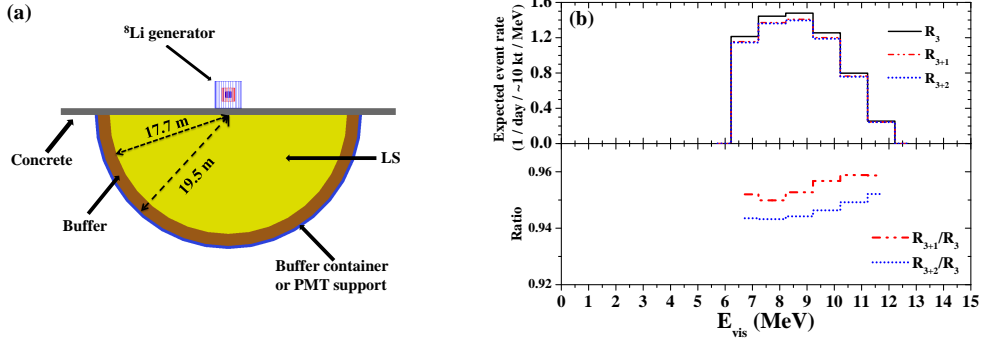


Figure 5. (Color online) (a) OpenGL picture showing simulation geometry for hemisphere type detector with ^8Li generator. (b) Expected event rates, R_3 , R_{3+1} and R_{3+2} by P_3 , P_{3+1} and P_{3+2} models, and their ratios with respect to E_{vis} . Here $6 \times 10^{11} \bar{\nu}_e/\text{s}$ from the setup III source with $T_1 = 43$ cm and $T_2 = 100$ cm by 1 g of ^{252}Cf is applied for the calculation.

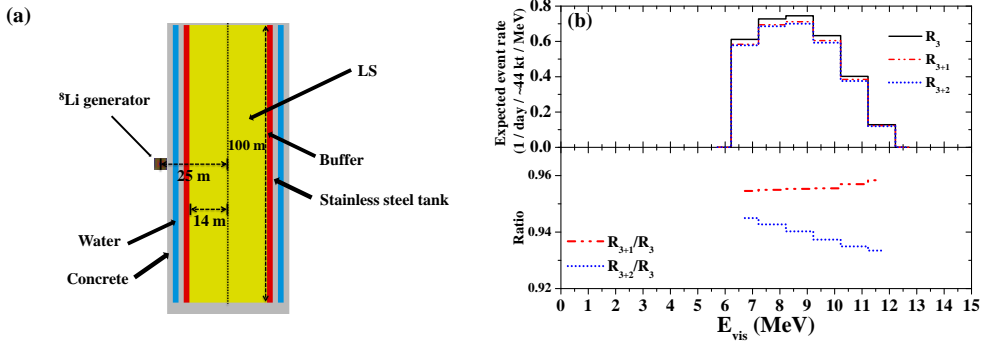


Figure 6. (Color online) Same as in Fig. 5 except that the detector has a cylinder shape.

First, a hemisphere shape scintillator detector based on the JUNO [23] is considered. The present proposed ^8Li generator requires the space of $T_1 = 43$ cm and $T_2 = 100$ cm in a detector. Thus, we consider a hemisphere shape of LS detectors with a radius of 17.7 m in Fig. 5(a) where the n_p in the detector is reduced to 0.725×10^{33} (~ 10 kt) [23]. The expected event rate is obtained within the hemisphere shape of LS detectors with the cylindrical setup III ^8Li generator. The evaluated event rates with P_3 , P_{3+1} and P_{3+2} , and their ratios are plotted in Fig. 5 (b). The ratios of R_{3+1}/R_3 and R_{3+2}/R_3 turns out to be ~ 0.955 and ~ 0.946 regardless of E_{vis} , respectively. These energy independent features can provide interesting results for the existence of a hypothetical ν_s .

The present proposed $\bar{\nu}_e$ source can also be useful for neutrino disappearance studies with future's gigantic LS detectors (LSDs) such as LENA (Low Energy Neutrino Astronomy) [25]. A 50 kt LSD LENA type detector would have specific features of low energy detection threshold, good energy resolution, and particle identification with efficient background discrimination [49, 50, 51]. The fiducial volume size for LENA is

Table 1. The key parameters used in this work.

Neutron source	^{252}Cf	
Neutron intensity	2.34×10^{12} n/s/g	
Neutrino production target	^7Li (99.99% enhanced) surrounded by graphite	
Run period	5 years	
$\bar{\nu}_e$ / neutron	0.256	
$\bar{\nu}_e$ flux	6×10^{11} $\bar{\nu}_e$ /s/g	
Neutrino energy cut	7 MeV ($E_{vis} = 6.22$ MeV)	
Detectors	hemisphere type	cylinder type
Fiducial mass	10 kt	44 kt
IBD event total	9750	4960

set to be 14 m in the radius and 100 m in the height [49], and 3.3×10^{33} target protons in the volume (44 kt) is assumed [25]. The ^8Li generator is placed at this LS detector as shown in Fig. 6(a). The expected event rates are obtained within the cylinder shape of LS LENA type detectors, whose values with P_3 , P_{3+1} and P_{3+2} and their ratios are plotted in Fig. 6(b). The ratios of R_{3+1}/R_3 are nearly constant with respect to E_{vis} . At the energies of $E_{vis} > 6$ MeV, however, the ratio of R_{3+2}/R_3 decreases as E_{vis} increases. The comparison between the ratios of R_{3+2}/R_3 and R_{3+1}/R_3 in this E_{vis} region can give a meaningful signal for distinguishing the 3+1 or 3+2 sterile neutrino scenarios. These characteristics are unique features of the present work due to the relatively higher energy of $\bar{\nu}_e$ ($E_{\bar{\nu}_e} < 13$ MeV) and the compact $\bar{\nu}_e$ source. ¶

The 95% C.L. sensitivities of the hemisphere and the cylinder type detectors with the ^8Li generator are obtained by following the Eq.(3) of Ref.[12] assuming 3% systematic uncertainty and 5% normalization uncertainty.⁺ The key parameters adopted for the sensitivity test are tabulated in Table 1, and whole results are plotted in Fig. 7, where we compared other sensitivities reported from Refs. [4, 10, 16]. For PROSPECT proposal [10], the High Flux Isotope Reactor (HFIR) [53] with a power of 85 MW and two neutrino detectors, AD-I and AD-II, were considered. And fiducialized target mass of 1.48 t (~ 7 t) and baseline range of 7 \sim 12 m (15 \sim 19 m) were assumed for AD-I (AD-II). The sensitivity of an accelerator-based IsoDAR by using ^8Li source [16] was obtained by considering a proton accelerator with a power of 600 kW, a fiducial target mass of 897 t and 16 m distance between the target face and the center of the KamLAND detector [24]. Here we exploited the following 2- ν oscillation survival probability

$$P = 1 - \sin^2(2\theta_{\text{new}})\sin^2\left(1.27\frac{\Delta m_{\text{new}}^2[\text{eV}^2]L[\text{m}]}{E[\text{MeV}]}\right), \quad (6)$$

¶ It is difficult to see the difference in Fig. 5(b) by the ^{144}Ce - ^{144}Pr antineutrino generators [13, 14] due to the low energy of $\bar{\nu}_e$ ($E_{\bar{\nu}_e} < 3$ MeV).

⁺ The ^8Li decays mainly to the broad 3.03 MeV, 2^+ level (first-excited state) of ^8Be , which then breaks up into two α particles [52]. Experimental ^8Li yields can be obtained by measuring ~ 3.03 MeV of typical gamma-rays peaks from the $^8\text{Be}^*$ in the ^8Li generator where the peak does not appear for the generator without Li.

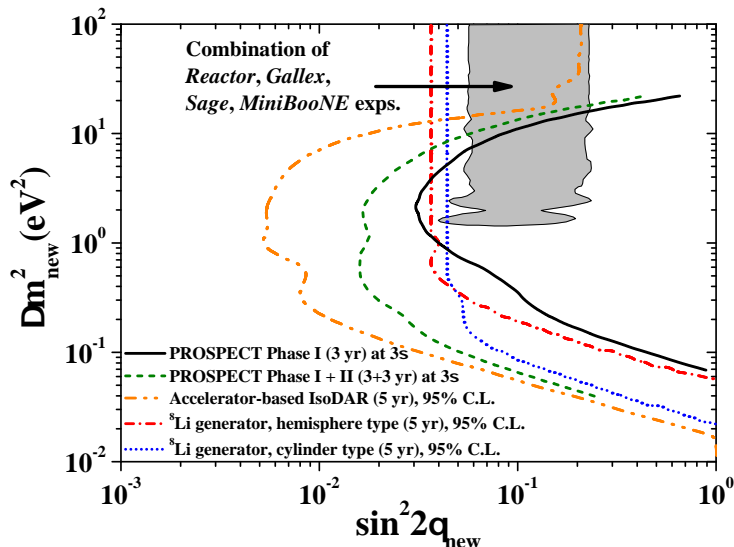


Figure 7. (Color online) 95% C.L. sensitivity of the hemisphere and the cylinder type detector with ^8Li generator proposed in this work. The gray area is an allowed region in the parameter space from the combination of reactor neutrino experiments, Gallex and Sage calibration sources experiments, and MiniBoone [4]. Sensitivities of PROSPECT (for Phase I and Phase II) [10] and an accelerator-based IsoDAR by using ^8Li source [16] are also plotted.

where θ_{new} and Δm_{new}^2 are the new oscillation parameters. When a five-years run with 1.5 g of ^{252}Cf is considered, the total expected events considering the effect of a half-life of ^{252}Cf and the neutrino energy cut of 7 MeV with P_3 are 9750 and 4960 for the hemisphere and the cylinder type detectors, respectively. The results in Fig. 7 clearly show that the proposed neutrino source can cover the region in parameter space from the reactor anomalies for the two LS detectors, and thus our scheme can be effectively used for testing the ν_s hypothesis [4].

In summary, $\bar{\nu}_e$ source by the ^8Li generator with the neutron emitter ^{252}Cf is compact so that neutrino detectors can be placed within a few meters from this neutrino source with $E_{\bar{\nu}_e} < 13$ MeV. Therefore, it is an efficient neutrino source for the study of 1 eV mass scale ν_s as well as other neutrino oscillation study. Two different types of experiments are considered. One is the hemisphere type detector, where the ^8Li generator is placed at the center of the detector. Another is to place the generator at the cylinder type detector. The shapes of event rates in Figs. 5(b) and 6(b) for the hemisphere and the cylinder type detectors can give effective chances to search for the existence of ν_s and to test the 3+1 or 3+2 sterile neutrino scenarios. If we can measure higher than or equal to 5% deviation from the expected events, in the case that the P_3 model is true, we can conclude which of the P_3 , P_{3+1} , and P_{3+2} models is the most appropriate scenario. Together with the reactor anomaly, our electron-antineutrino source can also be used for a precise test of the weak mixing angle at $\Delta m^2 \sim 1$ eV 2

order scale relevant to the sterile neutrino as shown in the sensitivity test results in Fig. 7.

Acknowledgments

The work of J. W. Shin is supported by the National Research Foundation of Korea (Grant No. NRF-2015R1C1A1A01054083), the work of M.-K. Cheoun is supported by the National Research Foundation of Korea (Grant No. NRF-2014R1A2A2A05003548 and NRF-2015K2A9A1A06046598).

References

- [1] Bellini G, Ludhova L, Ranucci G and Villante F L 2014 *Advances in High Energy Physics* **2014** 191960
- [2] Aguilar-Arevalo A *et al.* 2001 *Phys. Rev. D* **64** 112007 (The LSND collaboration)
- [3] Aguilar-Arevalo A *et al.* 2010 *Phys. Rev. Lett.* **105** 181801 (The MiniBooNE Collaboration)
- [4] Mention G, Fechner M, Lasserre T, Mueller T A, Lhuillier D, Cribier M and Letourneau A 2011 *Phys. Rev. D* **83** 073006
- [5] Giunti C and Laveder M 2011 *Phys. Rev. C* **83** 065504
- [6] Alekseev I *et al.* 2016 *JINST* **11** P11011
- [7] Serebrov A P *et al.* 2016 Neutrino-4 experiment on search for sterile neutrino with multi-section model of detector (*Preprint* 1605.05909)
- [8] Boireau G *et al.* 2016 *Phys. Rev. D* **93** 112006
- [9] Kuroda Y, Oguri S, Kato Y, Nakata R, Inoue Y, Ito C and Minowa M 2012 *Nucl. Instrum. Meth. A* **690** 41–47
- [10] Ashenfelter J *et al.* 2016 *J. Phys. G* **43** 113001
- [11] Abazajian K N *et al.* 2012 Light Sterile Neutrinos: A White Paper (*Preprint* 1204.5379)
- [12] Cribier M *et al.* 2011 *Phys. Rev. Lett.* **107** 201801
- [13] A Gando and others 2013 CeLAND: search for a 4th light neutrino state with a 3 PBq 144Ce-144Pr electron antineutrino generator in KamLAND (*Preprint* 1312.0896v2)
- [14] Bellini G *et al.* 2013 *JHEP* **2013** 38
- [15] Davison N E, Canty M J, Dohan D A and McDonald A 1974 *Phys. Rev. C* **10** 50–53
- [16] Bungau A, Adelmann A, Alonso J R, Barletta W, Barlow R, Bartoszek L, Calabretta L, Calanna A, Campo D, Conrad J M, Djurcic Z, Kamyshev Y, Shaevitz M H, Shimizu I, Smidt T, Spitz J, Wascko M, Winslow L A and Yang J J 2012 *Phys. Rev. Lett.* **109** 141802
- [17] Mikaelian L A, Spivak P E and Tsinoyev V G 1965 *Nucl. Phys.* **70** 574–576
- [18] An F P *et al.* 2016 *Phys. Rev. Lett.* **116** 061801 (The Daya Bay Collaboration)
- [19] Abe Y *et al.* 2014 *JHEP* **2014** 086
- [20] Kim S B 2013 *Nucl. Phys. B Proc. Suppl.* **235–236** 24–29
- [21] Seo S H 2015 *AIP Conf. Proc.* **1666** 080002 XXVI INTERNATIONAL CONFERENCE ON NEUTRINO PHYSICS AND ASTROPHYSICS: Neutrino 2014
- [22] Alimonti G *et al.* 2002 *Astropart. Phys.* **16** 205–234 (The Borexino Collaboration)
- [23] An F *et al.* 2016 *J. Phys. G* **43** 030401 (The JUNO Collaboration)
- [24] Abe S *et al.* 2008 *Phys. Rev. Lett.* **100** 221803 (The KamLAND Collaboration)
- [25] Wurm M *et al.* 2012 *Astropart. Phys.* **35** 685–732 (The LENA Collaboration)
- [26] Andringa S *et al.* 2016 *Advances in High Energy Physics* **2016** 6194250 (The SNO+ collaboration)
- [27] Watt B E 1952 *Phys. Rev.* **87** 1037
- [28] Smith A B, Fields P R and Roberts J H 1957 *Phys. Rev.* **108** 411

- [29] X-5 MONTE CARLO TEAM 2003 MCNP-A General Monte Carlo N-Particle Transport Code, Version 5 LA-UR-03-1987, Los Alamos National Lab.
- [30] Rubbia C 1997 Resonance enhanced neutron captures for element activation and waste transmutation. CERN-LHC/97-0040EET
- [31] Froment P, Tilquin I, Cogneau M, Delbar T, Vervier J and Ryckewaert G 2002 *Nucl. Instrum. Meth. A* **493** 165–175
- [32] Abbas K, Buono S, Burgio N, Cotogno G, Gibson N, Maciocco L, Mercurio G, Santagata A, Simonelli F and Tagziria H 2009 *Nucl. Instrum. Meth. A* **601** 223–228
- [33] Khorshidi A, Sadeghi M, Pazirandeh A, Tenreiro C and Kadi Y 2014 *J. Radioanal Nucl. Chem.* **299** 303–310
- [34] Agostinelli S *et al.* 2003 *Nucl. Instrum. Meth. A* **506** 250–303
- [35] Allison J *et al.* 2006 *IEEE Trans. Nucl. Sci.* **53** 270–278
- [36] ENDF/B-VII.1 Available online at <http://www.nndc.bnl.gov/csewg/>
- [37] Truscott P 2002 *Tech. Rep. Qinetiq* **60** 2966–2983
- [38] Hauf S, Kuster M, Batič M, Bell Z W, Hoffmann D H H, Lang P M, Neff S, Pia M G, Weidenspointner G and Zoglauer A 2013 *IEEE Trans. Nucl. Sci.* **60** 2966–2983
- [39] 2015 ENSDF Available online at <http://www.nndc.bnl.gov/ensdf/>
- [40] Möllenberg R 2013 *Monte Carlo study of solar ^8B neutrinos and the diffuse supernova neutrino background in LENA* PhD dissertation Technische Universität München Available online at <http://mediatum.ub.tum.de/doc/1175550/file.pdf>
- [41] de Gouvêa A and Jenkins J 2006 *Phys. Rev. D* **74** 033004
- [42] Strumia A and Vissani F 2003 *Phys. Lett. B* **564** 42–54
- [43] Strumia A and Vissani F 2010 Neutrino masses and mixings and ... (*Preprint hep-ph/0606054v3*)
- [44] Gonzalez-Garcia M C, Maltoni M, Salvado J and Schwetz T 2012 *JHEP* **2012** 123
- [45] Inoue K 2010 Neutrino 2010, Athen
- [46] Bellini G *et al.* 2010 *Phys. Lett. B* **687** 299–304 (The Borexino Collaboration)
- [47] Bellini G *et al.* 2013 *Phys. Lett. B* **722** 295–300 (The Borexino Collaboration)
- [48] Kopp J, Maltoni M and Schwetz T 2011 *Phys. Rev. Lett.* **107** 091801
- [49] Möllenberg R, von Feilitzsch F, Hellgartner D, Oberauer L, Tippmann M, Winter J, Wurm M and Zimmer V 2014 *Phys. Lett. B* **737** 251–255
- [50] Villante F L 2015 *Phys. Lett. B* **742** 279–284
- [51] Wurm M, Bick D, Enqvist T, Hellgartner D, Kaiser M, Loo K K, Lorenz S, Meloni M, Meyer M, Möllenberg R, Oberauer L, Soiron M, Smirnov M, Trzaska W H and Wonsak B 2015 *Phys. Procedia* **61** 376–383
- [52] Tilley D R, Kelley J H, Godwin J L, Millener D J, Purcell J E, Sheu C G and Weller H R 2004 *Nucl. Phys. A* **745** 155–362
- [53] High Flux Isotope Reactor <https://neutrons.ornl.gov/hfir>